Computational and Theoretical Chemistry 1084 (2016) 162–168

Contents lists available at ScienceDirect

Computational and Theoretical Chemistry

journal homepage: www.elsevier.com/locate/comptc

Assessment of different basis sets and DFT functionals for the calculation of structural parameters, vibrational modes and ligand binding energies of Zr_4O_2(carboxylate)$_{12}$ clusters

Johannes Kreutzer, Peter Blaha, Ulrich Schubert *

Institute of Materials Chemistry, Vienna University of Technology, Getreidemarkt 9, A-1060 Vienna, Austria

ARTICLE INFO

Article history:
Received 1 November 2015
Received in revised form 23 February 2016
Accepted 23 March 2016
Available online 24 March 2016

Keywords:
Clusters
Carboxylate ligands
Zirconium

ABSTRACT

Different basis sets and functionals in the framework of Density Functional Theory (DFT) were assessed for an accurate prediction of structural parameters and vibrational modes of the cluster Zr_4O_2(methacrylate)$_{12}$. A basis set of at least triple-ξ quality is necessary to accurately model the geometry and the IR spectra. Bond distances are best reproduced with hybrid functionals, while IR frequencies are best described by the generalized gradient approximation family of functionals. LDA functionals give the highest GGA functionals the lowest ligand binding energies. Increasing the amount of Hartree Fock exchange in the hybrid functionals results in higher binding energies. Binding energies of ligands in different positions of Zr_4O_2(methacrylate)$_{12}$ were calculated. The ligand binding energy decreases when the H atoms in an acetate ligand are successively replaced by F atoms with concomitant lengthening of the Zr–O bond. A chelating acetylacetonate ligand shows a higher ligand binding energy than chelating carboxylate ligands.

1. Introduction

Transition metal oxo clusters are often used as structurally well-defined nanosized building blocks for organic–inorganic hybrid materials [1–3]. Furthermore, clusters can be taken as model compounds for nanoparticles, particularly with regard to the stabilizing organic ligands bonded to the surface atoms. The surface science of nanoparticles [4,5] is much more difficult to investigate than that of clusters, where methods of molecular chemistry can be applied. Carboxylate-substituted clusters of the early transition metals are particularly well suited because they are easily prepared by reaction of metal alkoxides with carboxylic acids. Post-synthesis ligand exchange processes are an important means to modify the ligand shell of the clusters (or nanoparticles) for various reasons. The mechanism of ligand exchange reactions, especially that of anionic ligands, is less straightforward than that of molecular complexes [5]; such reactions therefore rely to a large extent on empirical evidence.

Particularly interesting would be site-selective ligand exchange for either blocking specific coordination sites or creating clusters with spatially directed functionalities. This is hampered by the fact that the ligands in many clusters are highly dynamic at room temperature. A rational approach for selective ligand exchange requires a better understanding of bonding in the clusters, especially prediction of metal–ligand bonds strength depending on the position of the metal at the cluster surface. To this end, different DFT basis sets and functionals were evaluated in this article with regard to an accurate description of the geometry of an oxo cluster, including positional and electronic effects of ligands. Vibrational spectra of the cluster core are one of the few possibilities to find out whether the cluster core was retained in a particular reaction. Assignment of the vibrational modes, however, is only possible by means of precise theoretical calculations [6].

The methacrylate-substituted cluster $Zr_4O_2(OMc)_{12}$ (OMc = methacrylate, **Zr4**) was chosen as a test case, because it is one of the best investigated and most often used oxo clusters due to its easy preparation and high stability. This includes crystal structure (CCDC 137083) [7], dynamic behavior in solution [8] and ligand exchange processes [6].

2. Computational details

All calculations were performed using the Gaussian09 [9] software package. Geometry optimizations of **Zr4** were performed with different functional/basis set combinations to check the reliability of DFT methods for correctly reproducing structural and vibrational parameters. Geometry optimization, starting from the experimental crystal structure [7], was performed without symmetry restrictions. The default convergence criteria set by the

* Corresponding author.
E-mail address: Ulrich.Schubert@tuwien.ac.at (U. Schubert).

http://dx.doi.org/10.1016/j.comptc.2016.03.030
2210-271X/

software Gaussian09 were applied in all geometry optimizations. Harmonic vibrations were calculated at the same level as the corresponding geometry and all vibrational energies are given in their unscaled form throughout the manuscript. Stationary points were characterized as minimum structures with all frequencies real.

Several functionals were considered, representing different types of exchange–correlation treatments. It was shown before that pure generalized gradient approximation (GGA) functionals tend to overestimate and local density approximation (LDA) functionals to underestimate bond lengths [10–12]. Each type of functional is included in this study. LDA is represented by the local-exchange-only functional Xα [13–15] (α = 0.7) and the local exchange correlation functional SVWN5 [13–16] and that of GGA by the OLYP [17–20] and PBE [21,22] functionals. The PBE functional was used for calculations on transition metal oxo clusters before [8]. The range of hybrid functionals is covered by the very successful PBE0 form [21–23] (25% Hartree Fock (HF) exchange), the one parameter hybrid functional mPW1PW91 [24] (25% HF exchange) and the well-known three parameter hybrid functional B3LYP [25] (20% HF exchange). TPSS [26] was chosen to represent the family of kinetic-energy density-dependent functionals (meta-GGA) and showed good performance for ligand binding energies in transition metal complexes and clusters before [27]. The CAM-B3LYP functional [28] (20–65% HF exchange), which behaves as a typical hybrid functional at short ranges but which adds up to 65% HF exchange at long ranges, was chosen to represent the family of long-range corrected functionals.

Different Gaussian type orbital (GTO) basis sets were used. The core electrons of the heavy atoms (Zr) were thereby modeled with relativistically corrected effective core potentials (ECP) in combination with the corresponding energy-optimized all electron basis sets for the valence electrons. Three different types of triple-ξ quality ECP's, namely LANL2TZ [29], SDD [30–32] and Def2TZVP [33], were tested. While all ECP treat 28 electrons in the core, they differ in the contraction scheme of the corresponding all electron basis sets. The additional polarization function renders the Def2TZVP basis (contraction scheme: (7s7p5d1f) → [6s4p3d1f]) the most flexible, followed by the SDD basis ((8s7p6d) → [6s5p3d]) and the LANL2TZ basis ((5s5p4d) → [5s5p3d]). The triple-ξ quality basis set TZVP from Ahlrichs was used for the light elements (C, H, O, F) [34]. The basis sets will be abbreviated as follows in the remainder of the article: LANL2TZ (LANL2TZ in combination with TZVP for the light elements); Def2TZVP (Def2TZVP in combination with TZVP for the light elements) and SDD (SDD in combination with TZVP for the light elements).

Additionally basis sets of double-ξ quality were used in a test run on geometry optimizations. The results showed that at least triple-ξ quality is necessary to obtain accurate results (MAE is between 0.03 Å and 0.06 Å for double-ξ quality and between 0.01 Å and 0.03 Å for triplet-ξ quality basis sets, depending on the functional), which is in agreement with previous findings [35].

The ligand binding energy is defined as the difference between the total energy of the optimized cluster and the total energies of the optimized cluster without the respective ligand and the free ligand [36]. Basis set superposition error (BSSE) effects were accounted for by the counterpoise method (CP) [37,38], as implemented in Gaussian09. All reported energies are relative energies and BSSE and zero-point energy (ZPE) corrected, unless otherwise noted. Relativistic effects are treated by using relativistically corrected ECPs.

3. Results and discussion

The structure of the centrosymmetric cluster $Zr_4O_2(OMc)_{12}$ (**Zr4**, Fig. 1) [7] consists of four coplanar Zr atoms, in which three

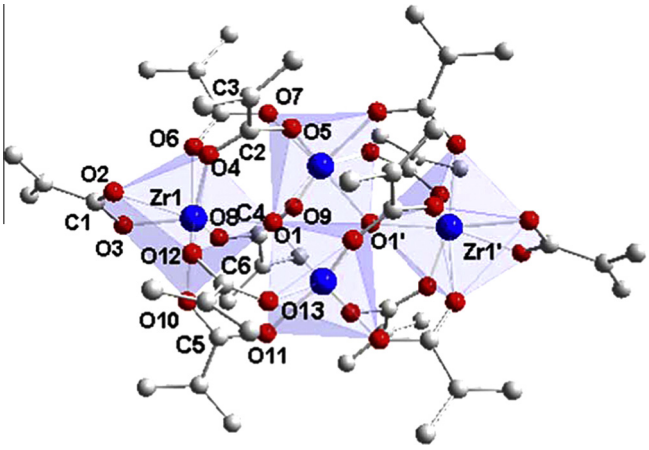

Fig. 1. Molecular structure of **Zr4**. Hydrogen atoms are omitted for clarity.

atoms each are connected through μ_3-oxo bridges and thus form a $[Zr_3O]$ triangle. The two atoms Zr1 and Zr1′ are coordinated by one chelating methacrylate ligand each while the remaining ten methacrylate ligands are bridging.

The crystallographic symmetry of **Zr4** (Fig. 1a) is C_i. An asymmetric structure was found in another structure determination [39], where one methacrylate ligand is chelating–bridging (μ_2, η^2). Experimental results showed previously, that the symmetric and asymmetric clusters easily interconvert in solution [7]. This was confirmed by theoretical calculations. The symmetric form of **Zr4** is 0.08 eV (1.91 kcal/mol) lower in energy than the asymmetric form (TPSS/Def2TZVP level of theory).

All calculations were performed on the symmetric structure **Zr4**. Geometry optimizations with the different basis sets and functionals usually took many steps to converge since the multidimensional potential energy surface is very shallow. The geometry optimizations nevertheless converged to comparable structures although symmetry restrictions were not applied during the optimization process and the default convergence criteria in Gaussian09 (see computational methods) were applied. The obtained minimum structures are all akin to the symmetric starting geometry of **Zr4** and retain the C_i symmetry during geometry optimization.

An assessment of different DFT methods to accurately reproduce the experimental geometry will be discussed first. It is based on the mean average error (MAE) of the most important bond lengths which include the bonds between the Zr atoms and the μ_3-O (O1) in the cluster core (Zr–μO), the bond lengths between Zr1 and the oxygen atoms of the chelating ligand ($Zr–O_c$) and the bond lengths between the Zr atoms and the oxygen atoms of the bridging ligands ($Zr–O_b$) relative to the experimental structure. The mean signed error (MSE) characterizes over- or underestimation of the calculated bond lengths. The root mean square deviation (RMS) with respect to the experimental structure of all these bond lengths was additionally used.

3.1. Basis set effect on cluster geometries

The accuracy generally increased when going from the least flexible LANL2TZ via SDD to the most flexible Def2TZVP basis set for all employed functionals. LDA functionals in combination with the Def2TZVP basis set consistently underestimated the bond lengths (MSE = −0.01 to −0.02 Å), an expected behavior of LDA functionals. In contrast, LDA functionals in combination with a limited basis set gave bond lengths which are longer than the experimental bond lengths (MSE = 0.01–0.03 Å). An exception

were Zr–O_b bond length calculated with XAlpha or SVWN in combination with the LANL2TZ basis set (MSE = −0.02 Å). In any case, LDA functionals gave shorter bond lengths than the other functionals with any basis set. Thus, decrease in flexibility of the basis set on the Zr atom results in greater bond lengths.

3.2. Functional effect on cluster geometries

Bond lengths generally decrease in the order GGA > meta-GGA ≈ Hybrid > LDA. The functionals were compared according to their MAE and RMS values for the three basis set combinations LANL2TZ, SDD and Def2TZVP and are shown in Figs. 2–5. The agreement of the structural results was particularly good with the hybrid functionals PBE0 and mPW1PW91 and the long range corrected functional CAM-B3LYP (RMS = 0.01 Å at the Def2TZVP level of theory). The pure GGA functionals, especially the OLYP functional, gave the worst results with RMS values exceeding 0.04 Å. Especially the metal–ligand bond lengths were, in the average, overestimated by 0.03–0.05 Å by this functional family. In general the hybrid functionals appeared superior to any other functional family when comparing the RMS values, with B3LYP as the only exception. However, including long range correction in the B3LYP functional form improved the results significantly. Thus, including HF exchange appears to be of uttermost importance for obtaining accurate geometrical parameters. The meta-GGA TPSS showed a balanced performance toward the different bonding situations in the cluster but dropped behind the hybrid functionals in terms of accuracy. This trend was found throughout all basis set combinations. Regarding the TPSS functional, the magnitude of error was smallest for the combination Def2TZVP. The method mPW1PW91 in combination with Def2TZVP gave the best agreement with the experiment. Experimental and calculated values obtained by mPW1PW91 in combination with Def2TZVP are shown in Table 1.

3.3. Functional effect on vibrational modes

Vibrational modes were calculated for all minimum structures obtained with the different functionals and compared with the experimental ATR spectrum [40]. All vibrational energies are given in their unscaled form throughout the manuscript and are given in Tables S1–S3 in the supplementary information. LDA, GGA and meta-GGA functionals resulted in the smallest deviation from the experiment, as can be seen from the low MSE values (Fig. 6) in the range of 20–40 cm^{-1}. Mixing with exact exchange increased the deviation, thus the hybrid functionals showed relatively high

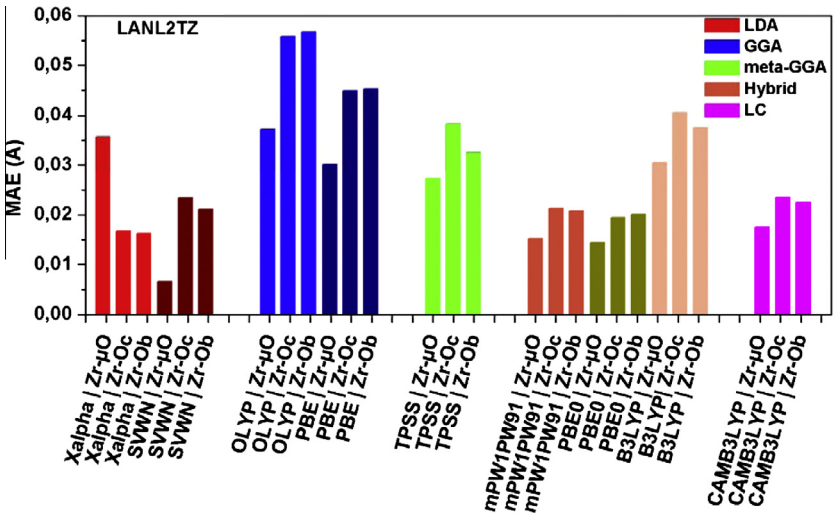

Fig. 2. MAE values [Å] of the geometry parameters depending on the different functionals. All calculations were performed with the LANL2TZ basis set.

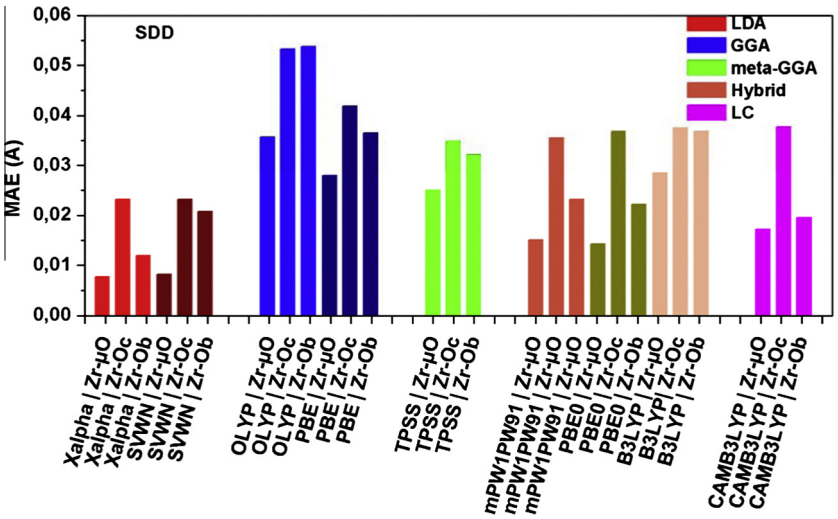

Fig. 3. MAE values [Å] of the geometry parameters depending on the different functionals. All calculations were performed with the SDD basis set.

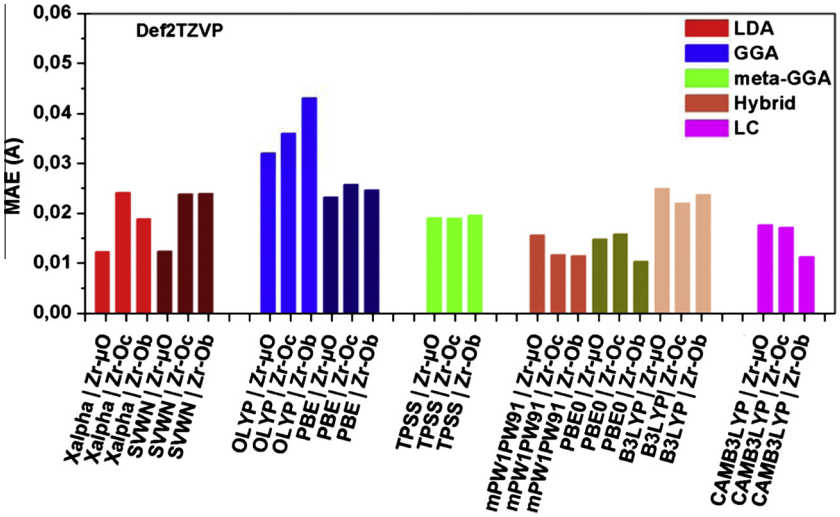

Fig. 4. MAE values [Å] of the geometry parameters depending on the different functionals. All calculations were performed with the Def2TZVP basis set.

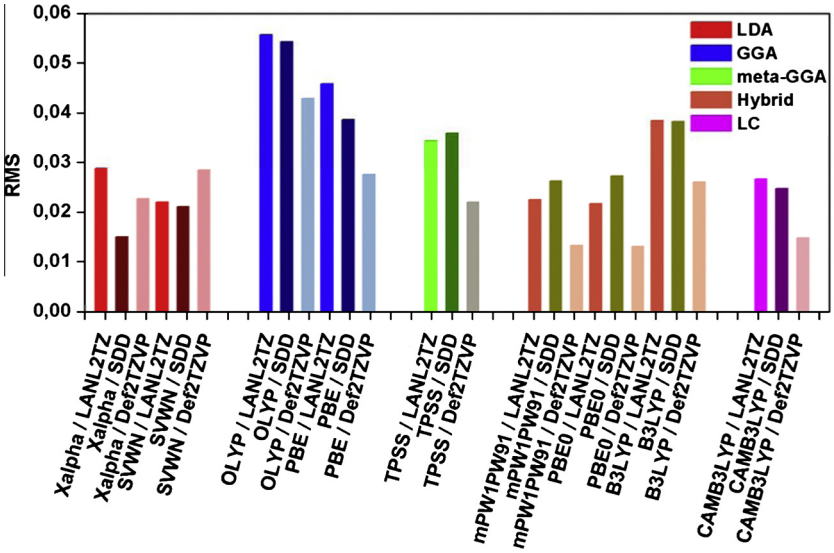

Fig. 5. RMS values of the geometry parameters for all optimized structures.

Table 1
Experimental [7] and calculated bond lengths (mPW1PW91/Def2TZVP level of theory).

	Type	Calc. (Å)	Exptl. (Å)		Type	Calc. (Å)	Exptl. (Å)
Zr1–O1	Zr–μO	2.086	2.065(2)	Zr2–O7	Zr–O_b	2.192	2.175(3)
Zr2–O1	Zr–μO	2.121	2.112(2)	Zr1–O8	Zr–O_b	2.229	2.218(3)
Zr2′–O1	Zr–μO	2.035	2.052(2)	Zr2–O9	Zr–O_b	2.176	2.166(2)
Zr1–O2	Zr–O_c	2.282	2.268(2)	Zr1–O10	Zr–O_b	2.204	2.201(3)
Zr1–O3	Zr–O_c	2.238	2.248(2)	Zr2′–O11	Zr–O_b	2.176	2.161(3)
Zr1–O4	Zr–O_b	2.207	2.224(3)	Zr1–O12	Zr–O_b	2.209	2.216(3)
Zr2–O5	Zr–O_b	2.179	2.174(3)	Zr2′–O13	Zr–O_b	2.186	2.171(3)
Zr1–O6	Zr–O_b	2.189	2.177(3)				

MSE values of >60 cm^{-1}. Two interesting points should be mentioned here: First, increasing the amount of HF exchange did not improve the accuracy. Both mPW1PW91 (25% exchange) and PBE0 (25% exchange) gave worse results than B3LYP (20% exchange). The long range corrected functional CAM-B3LYP performed equally bad as the mPW1PW91 and PBE0 functionals. Second, the accuracy of the results depended solely on the used functionals. A change of the basis set within one functional gave almost the same result with a maximum fluctuation of 5 cm^{-1} in the MIR and 30 cm^{-1} in the FIR region.

For a detailed analysis, the most remarkable vibrational modes were selected for comparison with experimental values, namely the asymmetric stretching-vibration of CH_3 (ν_{exptl} = 2978 cm^{-1}), the symmetric CH_3 stretching vibration (ν_{exptl} = 2926 cm^{-1}), the asymmetric stretching vibration of the bridging carboxylate ligands (ν_{exptl} = 1582, 1559 and 569 cm^{-1}), the symmetric stretching vibration of the bridging carboxylate ligands (ν_{exptl} = 1419, 1371 and 621 cm^{-1}) and the asymmetric (ν_{exptl} = 1495 cm^{-1}) and symmetric (ν_{exptl} = 1459 cm^{-1}) stretching vibration of the chelating carboxylate ligands. Furthermore the asymmetric deformation

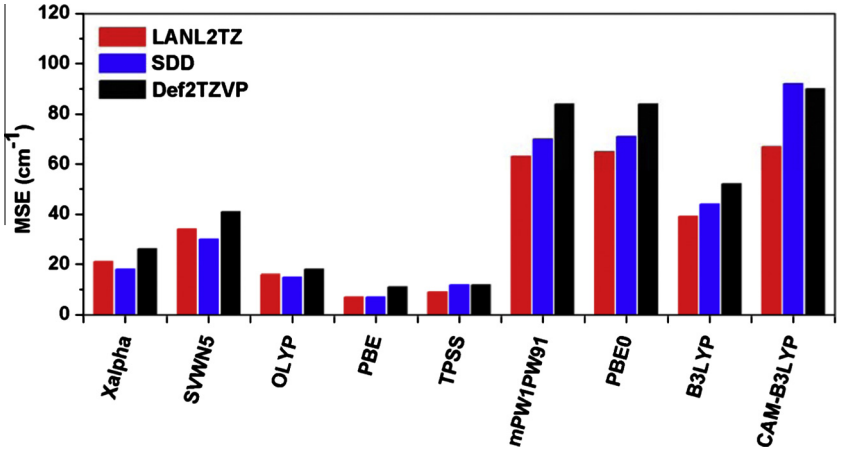

Fig. 6. MSE [cm^{-1}] of the vibrational modes depending on the different functionals.

Table 2
Experimental [40] and calculated IR frequencies (PBE1PBE/Def2TZVP level of theory).

Assignment	Exptl.	Calc.	Assignment	Exptl.	Calc.
ν_{as}(Me)	2978	3063	ν_s(COO)^b	1371	1379
ν_s(Me)	2926	2976	ν_s(COO)^b	621	623
ν_{as}(COO)^b	1582	1586	ν_{as}(COO)^b	569	585
ν_{as}(COO)^b	1559	1563	δ_s(μO–Zr)	520	540
ν_{as}(COO)^c	1495	1489	δ_{as}(μO–Zr)	292	279
ν_s(COO)^c	1459	1445	δ_s(μO–Zr)	247	253
ν_s(COO)^b	1419	1401			

b = bridging, c = chelating carboxylates; δ deformation vibration.

vibration of the $[Zr_4O_2]$ core (ν_{exptl} = 292 cm^{-1}) and the symmetric deformation vibration of the $[Zr_4O_2]$ core (ν_{exptl} = 520 and 247 cm^{-1}) were considered.

While the vibrational modes in the MIR region, which includes the carboxylate and methyl vibrations, were described with sufficient accuracy by all functionals (LDA and GGA showed ca. 1–5% overestimation and hybrid functionals ca. 5–10%), the $[Zr_4O_2]$ core deformation vibrations, mostly the asymmetric $[Zr_3–\mu O]$ vibration, were poorly reproduced by the hybrid functionals: mPW1PW91 and PBE0 both overestimated the asymmetric deformation vibration of the $[Zr_4O_2]$ core by 30% and CAM-B3LYP the asymmetric vibration by 53%. Overall, the choice of functional appears to be the most critical factor in correctly reproducing the vibrational modes. IR frequencies were best reproduced by the PBE functional in combination with the Def2TZVP basis set (Table 2). Experimental and calculated IR bands and MAE, MSE and MPE of the calculated IR bands are given in Table S4 of the supplementary information.

3.4. Effect of functionals on the HOMO–LUMO gap energies

HOMO–LUMO gap energies are very sensitive to the applied functional [41]. The HOMO–LUMO gap energy dependence on the functional (Table S5) followed the trend of previous reports [41,42], with LDA energies being the lowest at approximately 3.02 eV followed by the GGA functionals (ca. 3.2 eV). Including HF exchange increased the HOMO–LUMO gap energy in case of the hybrid functionals (5.17 eV B3LYP, 5.61 eV PBE0, 8.01 eV CAM-B3LYP). No absorption above 200 nm was observed in the experimental UV/VIS spectrum, i.e., the HOMO–LUMO gap energy must be higher than 6.2 eV. Applying different basis sets of one type, e.g. different basis sets of triple-ξ quality, did not impact the HOMO–LUMO gap energy. Thus, the magnitude of the HOMO–LUMO energy depended solely on the choice of the functional within one basis set series.

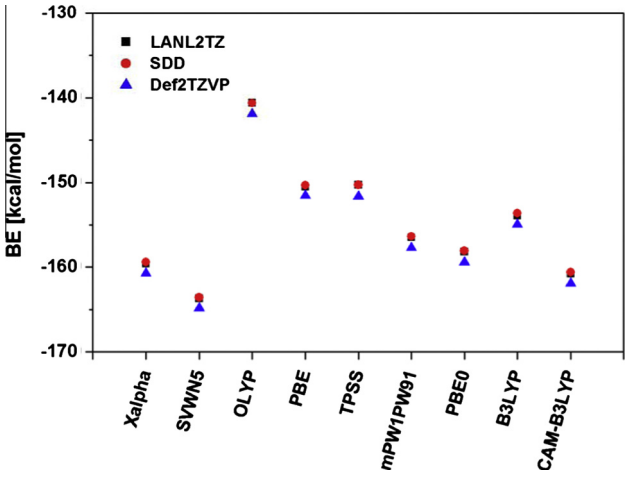

Fig. 7. Dependence of the ligand binding energies [kcal/mol] on the different functionals and core potentials.

3.5. Effect of basis set on the ligand binding energy

Ligand binding energies were calculated according to Ref. [36]. The dependence of ligand binding energies on the different basis set types and the functionals are shown in Fig. 7. Variations from LANL2TZ to SDD or Def2TZVP were small and within the range of 0.3–0.8 kcal/mol. LANL2TZ predicted generally the lowest binding energies. The ligand binding energies, however, were not very sensitive to changes in the Zr basis set and ECPs. The effect of CP correction was rather small; including CP decreased the binding energy by ca. 5 kcal/mol.

3.6. Effect of functionals on the ligand binding energy

The dependency of the ligand binding energies on the functional is much more pronounced (Fig. 7). The LDA functionals clearly predicted the highest binding energies (−160 to −165 kcal/mol). This is somehow expected, since a known drawback of LDA is to overestimate ligand binding energies [35]. GGA functionals and meta-GGA functionals decreased the ligand binding energies, with OLYP predicting the weakest binding energies (−142 kcal/mol). Increasing the amount of HF exchange in the hybrid functionals resulted in an increase of the ligand binding energy. The CAM-B3LYP functional predicted ligand binding energies (Table S6) close to the values obtained by the LDA functionals (−162 kcal/mol).

3.7. Dependence of ligand binding energy on ligand position in the cluster and the type of ligand

The assessment of the functionals and basis sets showed that the meta-GGA functional TPSS in combination with the Def2TZVP basis set and corresponding ECP for the Zr atoms and the TZVP basis set for the light atoms showed a balanced performance with regard to accurate prediction of geometries, vibrational frequencies and binding energies. All results reported in the following were therefore obtained by the TPSS Def2TZVP method. CP corrections showed only minor effects on the ligand binding energies but increased the computation time and were therefore not included in the calculation. The aim of this study was to model trends in ligand binding energies, rather than obtaining results at the highest level of accuracy.

In the first series (marked with a green box in Fig. 8), one methacrylate ligand, in different positions, was replaced with an acetate ligand. Position 1 corresponds to the chelating ligand (see Fig. 1). Positions 2–6 correspond to the bridging ligands as follows (see Fig. 1 for labeling of the C and O atoms): Pos. 2: O4–C2–O5; Pos. 3: O6–C3–O7; Pos. 4: O8–C4–O9; Pos. 5: O10–C5–O11; Pos. 6: O12–C6–O13.

Depending on the position, the binding energies for the acetate ligands are in the small range between −160 and −175 kcal/mol. The ligand in position 5 interacts most strongly with the metal (Table 3). There is no correlation between the bond lengths or angles and the binding energy for the ligands in different positions. It should be noted that the idealized molecular symmetry of **Zr4** is C_{2h} [8], where positions 2/4 and 5/6 would be pairwise equivalent (assuming that all ligands have the same configuration). The dynamic process with the lowest activation energy was previously found to be interchange of the chelating ligand (Pos. 1) with bridging OMc ligands in Pos. 2/4 [8]. As stated above, geometry optimization in the current work converged in an inversion-symmetric geometry (C_i) of **Zr4**.

The effect of electron-pulling substituents was also tested for the ligand in Pos. 3. The H atoms of the acetate ligand were thereby successively replaced by F atoms (blue box in Fig. 8). The ligand binding energy decreased in the series $CH_3 > CH_2F > CHF_2 > CF_3$. The biggest decrease (11 kcal/mol) was observed going from CH_3 to CH_2F, while further substitution to CHF_2 and CF_3 resulted in a decrease of 9 kcal/mol and 7 kcal/mol, respectively. This decrease of the binding energy correlated well with an increase of the bond lengths between the carboxy group and the Zr atom (Table 4).

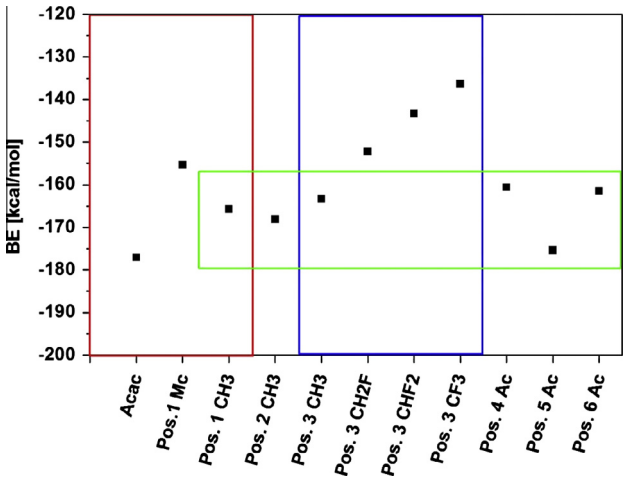

Fig. 8. Ligand binding energies [kcal/mol] of the acetate ligands (Ac) at different positions on the cluster (green box, see text for the definition of the positions). Ligand binding energies [kcal/mol] for the fluoro substituted acetate ligands (CFH_2, CF_2H, CF_3, blue box), and ligand binding energies [kcal/mol] for the chelating acetate, methacrylate and acetylacetonate ligands (red box). All calculations were performed with the TPSS functional in combination with the Def2TZVP basis set. (For interpretation of the references to color in this figure legend, the reader is referred to the web version of this article.)

Table 3
Ligand binding energies of the acetate ligands on different cluster positions, of different bridging carboxylate ligands in Pos. 3 and of chelating ligands in Pos. 1. For description of the positions see the text. All calculations were performed with the TPSS functional and the Def2TZVP basis set. Binding energies are not CP corrected.

Ligand	Cluster position	BE (kcal/mol)
Acetate	1	−165
Acetate	2	−168
Acetate	3	−163
Acetate	4	−160
Acetate	5	−175
Acetate	6	−161
Fluoroacetate	3	−152
Difluoroacetate	3	−143
Trifluoroacetate	3	−136
Methacrylate	1	−155
Acetylacetonate	1	−177

Table 4
Ligand binding energies of the $CH_{3-x}F_xCOO$ ligands (x = 0–3) in Pos. 3 (see the text for the description of the position). All calculations were performed with the TPSS functional and the Def2TZVP basis set. Binding energies are not CP corrected.

	Zr–O (Å)		BE (kcal/mol)
CH_3COO^-	2.19	2.14	−163
CH_2FCOO^-	2.21	2.26	−152
CHF_2COO^-	2.23	2.29	−143
CF_3COO^-	2.25	2.30	−136

Different chelating ligands were also investigated (red box in Fig. 8). Replacement of the chelating methacrylate by a chelating acetate ligand (Pos. 1) resulted in an increase of the binding energy by 10 kcal/mol. Replacement of the chelating carboxylate ligands by an acetylacetonate ligand resulted in further increase of the binding energy (12 kcal/mol compared to acetate, and 22 kcal/mol compared to methacrylate Table 3).

4. Conclusions

At least triple-ζ quality basis sets are needed to accurately describe the geometry of **Zr4**. The quality of the modeled structure increases with the flexibility of the basis set describing the Zr atoms. Shorter bond lengths are typically obtained with the most flexible Def2TZVP basis set. Within one basis set type, the geometry parameters depend significantly on the functionals: LDA and GGA tend to calculate too short or long bond lengths, respectively. Going from GGA to meta-GGA or hybrid functionals reduces the bond lengths and increases the accuracy.

On the other hand, LDA and GGA functionals generally perform better than hybrid functionals for the modeling of the vibrational modes. The latter tend to overestimate the vibrational modes by 5–10%. The performance on calculating vibrational modes depends mainly on the employed functional. Basis set effects are negligible. The meta-GGA TPSS and the GGA PBE show balanced results and perform best in this study.

According to the experimental UV/VIS spectrum of **Zr4**, the HOMO–LUMO gap energy must be higher than 6.2 eV and only calculations performed with hybrid functionals come close to 6 eV.

LDA functionals tend to give large and GGA functionals small binding energies. Increasing the amount of HF exchange in the functionals increases the binding energy; the results are similar to those obtained by the LDA functionals. The ligand binding energies of different cluster positions vary only little (ca. 15 kcal/mol) and do not correlate with the Zr–O bond length or the O–Zr–O

angles. This is different for electron-withdrawing substituents in the ligands. The ligand binding energy decreases when the H atoms in an acetate ligand are successively replaced by F atoms. The Zr–O bond lengths increase concomitantly. Replacing the chelating carboxylate ligand by acetylacetonate only results in a small increase of the binding energy, but favors the coordination of the acetylacetonate ligand. Differences in the binding energies on the different cluster positions, as well as substituent effects are small and explain the experimental result that ligand exchange reactions result in a random exchange of the carboxylate ligands. The theoretical results are in agreement with the known dynamic behavior of the ligands.

Acknowledgements

This work was supported by the *Fonds zur Förderung der Wissenschaftlichen Forschung* (FWF), Austria (projects P22915 and W1243). Calculations were done at the Vienna Scientific Cluster (VSC).

Appendix A. Supplementary material

Supplementary data associated with this article can be found, in the online version, at http://dx.doi.org/10.1016/j.comptc.2016.03.030.

References

[1] U. Schubert, Chem. Mater. 13 (2001) 3487.
[2] L. Rozes, C. Sanchez, Chem. Soc. Rev. 40 (2011) 1006.
[3] U. Schubert, Chem. Soc. Rev. 40 (2011) 575.
[4] M.-A. Neouze, U. Schubert, Monatsh. Chem. 139 (2008) 183.
[5] M.A. Boles, D. Ling, T. Hyeon, D.V. Talapin, Nat. Mater. 15 (2016) 141.
[6] J. Kreutzer, X.-H. Qin, C. Gorsche, H. Peterlik, R. Liska, U. Schubert, Mater. Today Commun. 5 (2015) 10.
[7] G. Trimmel, S. Gross, G. Kickelbick, U. Schubert, Appl. Organomet. Chem. 15 (2001) 401.
[8] P. Walther, M. Puchberger, F.R. Kogler, K. Schwarz, U. Schubert, Phys. Chem. Chem. Phys. 11 (2009) 3640.
[9] G.W.T.M.J. Frisch, H.B. Schlegel, G.E. Scuseria, M.A. Robb, J.R. Cheeseman, G. Scalmani, V. Barone, B. Mennucci, G.A. Petersson, H. Nakatsuji, M. Caricato, X. Li, H.P. Hratchian, A.F. Izmaylov, J. Bloino, G. Zheng, J.L. Sonnenberg, M. Hada, M. Ehara, K. Toyota, R. Fukuda, J. Hasegawa, M. Ishida, T. Nakajima, Y. Honda, O. Kitao, H. Nakai, T. Vreven, J.A. Montgomery Jr., J.E. Peralta, F. Ogliaro, M. Bearpark, J.J. Heyd, E. Brothers, K.N. Kudin, V.N. Staroverov, R. Kobayashi, J. Norm, K. Raghavachari, A. Rendell, J.C. Burant, S.S. Iyengar, J. Tomasi, M. Cossi, N. Rega, J.M. Millam, M. Klene, J.E. Knox, J.B. Cross, V. Bakken, C. Adamo, J. Jaramillo, R. Gomperts, R.E. Stratmann, O. Yazyev, A.J. Austin, R. Cammi, C. Pomelli, J.W. Ochterski, R.L. Martin, K. Morokuma, V.G. Zakrzewski, G.A. Voth, P. Salvador, J.J. Dannenberg, S. Dapprich, A.D. Daniels, Ö. Farkas, J.B. Foresman, J. V. Ortiz, J. Cioslowski, D.J. Fox, Wallingfort CT, Edition 2009.
[10] N. Rösch, V.A. Nasluzov, Chem. Phys. 210 (1996) 415.
[11] O.D. Häberln, C.-S. Chung, M. Stener, N. Rösch, J. Chem. Phys. 106 (1997) 5189.
[12] C.M. Aikens, J. Phys. Chem. A 113 (2009) 10811.
[13] P. Hohenberg, W. Kohn, Phys. Rev. 136 (1964) B864.
[14] W. Kohn, L.J. Sham, Phys. Rev. 140 (1965) A1133.
[15] J.C. Slater, The Self-Consistent Field for Molecular and Solids, Quantum Theory of Molecular and Solids, vol. 4, McGraw-Hill, New York, 1974.
[16] S.H. Vosko, L. Wilk, M. Nusair, Can. J. Phys. 58 (1980) 1200.
[17] N.C. Hy, A.J. Cohen, Mol. Phys. 99 (2001) 403.
[18] W.-M. Hoe, A. Cohen, N.C. Hy, Chem. Phys. Lett. 341 (2001) 319.
[19] C. Lee, W. Yang, R.G. Parr, Phys. Rev. B 37 (1988) 785.
[20] B. Miehlich, A. Savin, H. Stoll, H. Preuss, Chem. Phys. Lett. 157 (1989) 200.
[21] J.P. Perdew, K. Burke, M. Ernzerhof, Phys. Rev. Lett. 77 (1996) 3865.
[22] J.P. Perdew, K. Burke, M. Ernzerhof, Phys. Rev. Lett. 78 (1997) 1396.
[23] C. Adamo, V. Barone, J. Chem. Phys. 110 (1999) 6158.
[24] C. Adamo, V. Barone, J. Chem. Phys. 108 (1998) 664.
[25] A.D. Becke, J. Chem. Phys. 98 (1993) 5648.
[26] J.M. Tao, J.P. Perdew, V.N. Staroverov, G.E. Scuseria, Phys. Rev. Lett. 91 (2003) 146401.
[27] C.J. Cramer, D.G. Truhlar, Phys. Chem. Chem. Phys. 11 (2009) 10757.
[28] T. Yanai, D. Tew, N. Hy, Chem. Phys. Lett. 393 (2004) 51.
[29] P.J. Hay, W.R. Wadt, J. Chem. Phys. 82 (1985) 299.
[30] A. Bergner, M. Dolg, W. Kuechle, H. Stoll, H. Preuss, Mol. Phys. 80 (1993) 1431.
[31] M. Kaupp, P.V.R. Schleyer, H. Stoll, H. Preuss, J. Chem. Phys. 94 (1991) 1360.
[32] M. Dolg, H. Stoll, H. Preuss, R.M. Pitzer, J. Phys. Chem. 97 (1993) 5852.
[33] W. Weigend, R. Ahlrichs, Phys. Chem. Chem. Phys. 7 (2005) 3297.
[34] A. Schaefer, C. Huber, R. Ahlrichs, J. Chem. Phys. 100 (1994) 5829.
[35] V.V. Albert, S.A. Ivanov, S. Tretiak, S.V. Kilina, J. Phys. Chem. C 115 (2011) 15793.
[36] S.A. Ivanov, I. Arachchige, C.M. Aikens, J. Phys. Chem. A 115 (2011) 8017.
[37] S.F. Boys, F. Bernardi, Mol. Phys. 19 (1970) 553.
[38] S. Simon, M. Duran, J.J. Dannenberg, J. Chem. Phys. 105 (1996) 11024.
[39] G. Kickelbick, U. Schubert, Chem. Ber. 130 (1997) 473.
[40] J. Kreutzer, M. Puchberger, C. Artner, U. Schubert, Eur. J. Inorg. Chem. (2015) 2145.
[41] J. Muscat, A. Wander, N.M. Harrison, Chem. Phys. Lett. 342 (2001) 397.
[42] S. Tretiak, K. Igumenschev, V. Chernyak, Phys. Rev. B 71 (2005) 33201.